IEEE Access
Multidisciplinary | Rapid Review | Open Access Journal

Received February 26, 2022, accepted March 30, 2022, date of publication April 6, 2022, date of current version April 14, 2022.

Digital Object Identifier 10.1109/ACCESS.2022.3165200

Toward Quaternary QCA: Novel Majority and XOR Fuzzy Gates

REZA AKBARI-HASANJANI[1], REZA SABBAGHI-NADOOSHAN[1,2], AND MAJID HAGHPARAST[3]

[1]Department of Electrical Engineering, Central Tehran Branch, Islamic Azad University, Tehran 14696-69191, Iran
[2]School of Computer Science, Institute for Research in Fundamental Sciences (IPM), Tehran 19538-33511, Iran
[3]Faculty of Information Technology, University of Jyväskylä, FI-40014 University of Jyväskylä, Jyväskylä, Finland

Corresponding author: Majid Haghparast (majid.m.haghparast@jyu.fi)

This work was supported by the University of Jyväskylä (JYU) for Open Access.

ABSTRACT As an emerging nanotechnology, quantum-dot cellular automata (QCA) has been considered an alternative to CMOS technology that suffers from problems such as leakage current. Moreover, QCA is suitable for multi-valued logic due to the simplicity of implementing fuzzy logic in a way much easier than CMOS technology. This paper uses a quaternary cell with two isolated layers because of requiring three particles to design this quaternary cell. Moreover, due to the instability of the basic gates, the three particles cannot be placed in one layer. The first layer of the proposed two-layer cell includes a ternary cell and the second one includes a binary cell. It is assumed that the overall polarization of the quaternary QCA (QQCA) cell is determined as the combined polarization of the two layers. The proposed QQCA cell can also be implemented in one layer. Simulations of the QQCA cell are performed based on analytical calculations. Moreover, a majority fuzzy gate, an XOR fuzzy gate, and a crossbar structure are simulated.

INDEX TERMS Multi-valued QCA, majority fuzzy gate, XOR fuzzy gate, quaternary, polarization, QQCA.

I. INTRODUCTION

Quantum-dot cellular automata (QCA) technology is a candidate to replace CMOS technology in digital circuit designs. CMOS technology has encountered some problems because of the technology scaling. According to Moore's law, the component density of integrated circuits doubles every two years, so scaling of transistors and the subsequent problems in circuit implementation are inevitable [1]–[8]. QCA, which implementation is by Lent *et al.* in the 1990s, is a promising approach for future computing systems with optimal reliability and performance [2], [4], [9]. Data transfer in QCA cells is based on quantum effects and external electrostatic fields, and no current is transferred in QCA-based circuits. Instead, data is transmitted from one cell to another based on the polarization of cells [1], [2].

The first designed binary QCA (bQCA) model contained four potential wells and two electrons [9]–[13]. The second electron in a bQCA cell stabilizes the cell [14]–[19]. The first multiple-valued logic (MVL) design in QCA was the ternary QCA, which consisted of eight potential wells and two electrons [1]–[3], [20]–[27].

The associate editor coordinating the review of this manuscript and approving it for publication was Giovanni Pau.

Multiple-valued logic has drawn attention because of its similarity to fuzzy logic and natural variable description. The advantages of using MVL are reducing the number of inputs/outputs, high speed, simplicity, and cost-efficiency. Moreover, MVL can be applied to provide more information on system variables [1], [3].

Many studies have been conducted on ternary cells to design basic gates. However, a QCA cell with more than three values has not been presented. This paper presents a quaternary QCA (QQCA) cell for quantum computation.

II. QQCA

This section presents a QQCA cell model as a three-particle (electron) system. In this system, the electron spin value is equal to 1/2, the quantum number of an electron can be 1/2 or −1/2 [28], and the quantum states describe a three-particle system.

A. BACKGROUND OF QQCA QUANTUM COMPUTING

This section will briefly discuss the concepts of the Hamiltonian matrix and the calculation of polarization in QQCA. As mentioned, each QQCA system can be considered a three-particle system with eight different states based on the

quantum number of the particles. Using these quantum states, a state matrix can be provided for the system as given in Eq. 1., as shown at the bottom of the page. Moreover, Eq. 1 expresses all states and the spin effect of the particles on each other. This matrix can be separated into three states, each representing the state of a particle. Following the separation of the states, the spin angular momentum in the x, y, and z directions can be calculated for each particle from Eqs. 2 to 4 [20], [28].

$$S_z = < j, m' | j_z | j, m >= \hbar m \delta_{j',j} \delta_{m',m} \tag{2}$$

$$S_x = \frac{1}{2}((\hbar\sqrt{j(j+1) - m(m+1)}\delta_{j',j}\delta_{m',m+1}) + (\hbar\sqrt{j(j+1) - m(m-1)}\delta_{j',j}\delta_{m',m-1})) \tag{3}$$

$$S_y = \frac{i}{2}((\hbar\sqrt{j(j+1) - m(m-1)}\delta_{j',j}\delta_{m',m-1}) - (\hbar\sqrt{j(j+1) - m(m+1)}\delta_{j',j}\delta_{m',m+1})) \tag{4}$$

In the scheme, the calculations are performed for a three-particle system. The calculated spin angular momenta in the three directions for each particle (based on Eq. 1) are algebraically summed, as given in Eqs. 5 to 7.

$$S_x = S_{1x} + S_{2x} + S_{3x} \tag{5}$$

$$S_y = S_{1y} + S_{2y} + S_{3y} \tag{6}$$

$$S_z = S_{1z} + S_{2z} + S_{3z} \tag{7}$$

Based on Eqs. 5 to 7, the spin angular momentum in the x, y, and z directions can be written as follows [28]:

$$S_x = \frac{\hbar}{2}\begin{bmatrix} 0 & 1 & 1 & 2 & 1 & 2 & 2 & 3 \\ 1 & 0 & 2 & 1 & 2 & 1 & 3 & 2 \\ 1 & 2 & 0 & 1 & 2 & 3 & 1 & 2 \\ 2 & 1 & 1 & 0 & 3 & 2 & 2 & 1 \\ 1 & 2 & 2 & 3 & 0 & 1 & 1 & 2 \\ 2 & 1 & 3 & 2 & 1 & 0 & 2 & 1 \\ 2 & 3 & 1 & 2 & 1 & 2 & 0 & 1 \\ 3 & 2 & 2 & 1 & 2 & 1 & 1 & 0 \end{bmatrix}$$

$$S_y = \frac{\hbar}{2}\begin{bmatrix} 0 & -i & -i & -2i & -i & -2i & -2i & -3i \\ i & 0 & 0 & -i & 0 & -i & -i & -2i \\ i & 0 & 0 & -i & 0 & -i & -i & -2i \\ 2i & i & i & 0 & i & 0 & 0 & -i \\ i & 0 & 0 & -i & 0 & -i & -i & -2i \\ 2i & i & i & 0 & i & 0 & 0 & -i \\ 2i & i & i & 0 & i & 0 & 0 & -i \\ 3i & 2i & 2i & i & 2i & i & i & 0 \end{bmatrix}$$

$$S_z = \frac{\hbar}{2}\begin{bmatrix} 3 & 2 & 2 & 1 & 2 & 1 & 1 & 0 \\ 2 & 1 & 1 & 0 & 1 & 0 & 0 & -1 \\ 2 & 1 & 1 & 0 & 1 & 0 & 0 & -1 \\ 1 & 0 & 0 & -1 & 0 & -1 & -1 & -2 \\ 2 & 1 & 1 & 0 & 1 & 0 & 0 & -1 \\ 1 & 0 & 0 & -1 & 0 & -1 & -1 & -2 \\ 1 & 0 & 0 & -1 & 0 & -1 & -1 & -2 \\ 0 & -1 & -1 & -2 & -1 & -2 & -2 & -3 \end{bmatrix}$$

By eliminating $\frac{\hbar}{2}$ from S_x, S_y, and S_z, the value of δ is obtained in three directions. Another problem in QCA-based cells is the calculation of the Hamiltonian matrix. In QCA technology, the Hamiltonian matrix is determined using the Hartree-Fock approximation as given in Eq. 8.

$$\hat{H}_j = -\gamma_j \delta_x(j) - \frac{E_k}{2}\delta_z(j) P_j \tag{8}$$

where γ_j is the tunneling energy; $\delta_x(j)$ and $\delta_z(j)$ are the quasi-Pauli matrices in the x- and z-directions, respectively; P_j is the polarization of QQCA, and E_k is the kink energy value. Using Eq. 8, the value of the Hamiltonian matrix in QQCA can be obtained as described in [28], $\hat{H}_j$, as shown at the bottom of the next page. In this scheme, quantum measurements are required to calculate the polarization of the input state) from $\delta_z(j)$ in the z-direction) as performed in Eq. 9 [20], [28].

$$P_k = -\langle \delta_{zk} \rangle \tag{9}$$

For the quantum calculations and measurements, the input states must be specified. For the three particles, there are eight states. States $|\rangle$ and $|\rangle$ are shown in the following, but all input

$$S = \begin{bmatrix} \langle \frac{1}{2},\frac{1}{2};\frac{1}{2},\frac{1}{2};\frac{1}{2},\frac{1}{2}|S|\frac{1}{2},\frac{1}{2};\frac{1}{2},\frac{1}{2};\frac{1}{2},\frac{1}{2}\rangle & \cdots & \cdots & \langle \frac{1}{2},\frac{1}{2};\frac{1}{2},\frac{1}{2};\frac{1}{2},\frac{1}{2}|S|\frac{1}{2},-\frac{1}{2};\frac{1}{2},-\frac{1}{2};\frac{1}{2},-\frac{1}{2}\rangle \\ \langle \frac{1}{2},\frac{1}{2};\frac{1}{2},\frac{1}{2};\frac{1}{2},-\frac{1}{2}|S|\frac{1}{2},\frac{1}{2};\frac{1}{2},\frac{1}{2};\frac{1}{2},\frac{1}{2}\rangle & \cdots & \cdots & \langle \frac{1}{2},\frac{1}{2};\frac{1}{2},\frac{1}{2};\frac{1}{2},-\frac{1}{2}|S|\frac{1}{2},-\frac{1}{2};\frac{1}{2},-\frac{1}{2};\frac{1}{2},-\frac{1}{2}\rangle \\ \vdots & & & \vdots \\ \langle \frac{1}{2},-\frac{1}{2};\frac{1}{2},-\frac{1}{2};\frac{1}{2},\frac{1}{2}|S|\frac{1}{2},\frac{1}{2};\frac{1}{2},\frac{1}{2};\frac{1}{2},\frac{1}{2}\rangle & \cdots & \cdots & \langle \frac{1}{2},-\frac{1}{2};\frac{1}{2},-\frac{1}{2};\frac{1}{2},\frac{1}{2}|S|\frac{1}{2},-\frac{1}{2};\frac{1}{2},-\frac{1}{2};\frac{1}{2},-\frac{1}{2}\rangle \\ \langle \frac{1}{2},-\frac{1}{2};\frac{1}{2},-\frac{1}{2};\frac{1}{2},-\frac{1}{2}|S|\frac{1}{2},\frac{1}{2};\frac{1}{2},\frac{1}{2};\frac{1}{2},\frac{1}{2}\rangle & \cdots & \cdots & \langle \frac{1}{2},-\frac{1}{2};\frac{1}{2},-\frac{1}{2};\frac{1}{2},-\frac{1}{2}|S|\frac{1}{2},-\frac{1}{2};\frac{1}{2},-\frac{1}{2};\frac{1}{2},-\frac{1}{2}\rangle \end{bmatrix}_{8*8} \tag{1}$$

states are considered in the calculations.

$$|000\rangle = \begin{bmatrix} 0 \\ 0 \\ 0 \\ 0 \\ 0 \\ 0 \\ 0 \\ 1 \end{bmatrix} \quad |111\rangle = \begin{bmatrix} 1 \\ 0 \\ 0 \\ 0 \\ 0 \\ 0 \\ 0 \\ 0 \end{bmatrix}$$

Based on the quantum measurements of input state matrices, the polarization value are $\{-3, -1, -1, 1, -1, 1, 1, 3\}$. In the next section, a two-layer QQCA cell is presented. This cell can also be presented in one layer. The QQCA cell uses a bQCA cell and a ternary QCA (tQCA) cell, which are separated by a distance of 25 nm.

Four particles exist in the QQCA cell. The tQCA cell has two electrons that can provide the polarization $\{-2\ 0\ 0\ 2\}$, and the bQCA cell has another two electrons and four potential wells. However, the bQCA cell can also include a single particle as used in [14]–[19]. Because four potential wells exist in the bQCA cell of the QQCA cell, the second electron is considered for cell stability. Moreover, to obtain the Hamiltonian matrix of the bQCA cell, it must be considered as a single particle system as given in Eq. 10 [27], [29]–[34].

$$H(j) = \begin{bmatrix} -\frac{E_k}{2}P_j & -\gamma j \\ -\gamma j & \frac{E_k}{2}P_j \end{bmatrix} \tag{10}$$

The polarization of the QQCA cell contributes to the polarizations of the bQCA and tQCA cells.

B. SUGGESTED QQCA CELL

Quaternary logic increases the speed, requires fewer inputs/outputs, reduces circuit complexity, and allows cost-effective implementation.

A quaternary system requires three particles (electrons) to produce four different polarizations. The polarizations are calculated by solving Eq. (1) and performing quantum measurements in the z-direction, and finally, the polarization values $\{-3, -1, -1, 1, -1, 1, 1, 3\}$ are achieved. Some of the polarizations are duplicated, which are ignored in this study, so the polarizations of the QQCA system are $\{-3, -1, 1, 3\}$ [28].

The quaternary system consists of three particles, which lead to instability in the gate if they are placed in one layer.

Therefore, the QQCA cell is presented in two layers, which are separated by 25 nm to reduce and eliminate the electrostatic effects between these two isolated layers. The first layer of the QQCA cell contains a tQCA cell with the polarization $\{-2\ 0\ 0\ 2\}$ from which only -2 and 2 are chosen. The second layer contains a bQCA cell with the polarization $\{-1\ 1\}$ [20], [28].

To fabricate QCA cells, electron beam lithography with two resist layers on Si or Si/SiO2 substrate is used, and quantum dots are deposited on an aluminum substrate, as explained in [35].

The QQCA cell structure can also be implemented on one layer. The dimensions of less than 10 nm can be achieved using some methods, such as field emission scanning probe (FE-SP) [36], plasmonic lithography [37], electron beam lithography using polymethylmethacrylate (PMMA) resist [38], and extreme ultraviolet (EUV) interference lithography [39].

In [40], a bQCA cell is fabricated with four quantum dots and two electrons with dimensions of 6 nm×6 nm using Si (100) dangling bonds (DBs). In [41], a bQCA cell is fabricated with two quantum dots and one electron with dimensions of 2 nm using Si DBs.

Figure 1(a) shows the model of the cell in [28], and Figure 1(b) shows the dimensions of the layers [28]. The QQCA model is a three-dimensional structure, so it is difficult to show the designed quaternary gates that use this model. For this reason, the symbolic model is used in the simulation. Figure 1(c) shows the QQCA cell symbol [28]. The QQCA cell polarization consists of the polarizations of both the first (ternary) and the second (binary) layers. Figure 1(d) shows the polarizations of the QQCA cell [28].

III. INTEGRATION IN APPLYING INPUTS TO THE QQCA CELL

In the QQCA structure, the input to the cell in each layer is applied through single-electron transistors (SETs). Thus, the input can be integrated into the cell using digital circuits.

$$\hat{H}_j = \begin{bmatrix}
-\frac{3}{2}E_kP_j & -E_kP_j-\gamma_j & -E_kP_j-\gamma_j & -\frac{1}{2}E_kP_j-2\gamma_j & -E_kP_j-\gamma_j & -\frac{1}{2}E_kP_j-2\gamma_j & -\frac{1}{2}E_kP_j-2\gamma_j & -3\gamma_j \\
-E_kP_j-\gamma_j & -\frac{1}{2}E_kP_j & -\frac{1}{2}E_kP_j-2\gamma_j & -\gamma_j & -\frac{1}{2}E_kP_j-2\gamma_j & -\gamma_j & -3\gamma_j & \frac{1}{2}E_kP_j-2\gamma_j \\
-E_kP_j-\gamma_j & -\frac{1}{2}E_kP_j-2\gamma_j & -\frac{1}{2}E_kP_j & -\gamma_j & -\frac{1}{2}E_kP_j-2\gamma_j & -3\gamma_j & -\gamma_j & \frac{1}{2}E_kP_j-2\gamma_j \\
-\frac{1}{2}E_kP_j-2\gamma_j & -\gamma_j & -\gamma_j & \frac{1}{2}E_kP_j & -3\gamma_j & \frac{1}{2}E_kP_j-2\gamma_j & \frac{1}{2}E_kP_j-2\gamma_j & E_kP_j-\gamma_j \\
-E_kP_j-\gamma_j & -\frac{1}{2}E_kP_j-2\gamma_j & -\frac{1}{2}E_kP_j-2\gamma_j & -3\gamma_j & -\frac{1}{2}E_kP_j & -\gamma_j & -\gamma_j & \frac{1}{2}E_kP_j-2\gamma_j \\
-\frac{1}{2}E_kP_j-2\gamma_j & -\gamma_j & -3\gamma_j & \frac{1}{2}E_kP_j-2\gamma_j & -\gamma_j & \frac{1}{2}E_kP_j & \frac{1}{2}E_kP_j-2\gamma_j & E_kP_j-\gamma_j \\
-\frac{1}{2}E_kP_j-2\gamma_j & -3\gamma_j & -\gamma_j & \frac{1}{2}E_kP_j-2\gamma_j & -\gamma_j & \frac{1}{2}E_kP_j-2\gamma_j & \frac{1}{2}E_kP_j & E_kP_j-\gamma_j \\
-3\gamma_j & \frac{1}{2}E_kP_j-2\gamma_j & \frac{1}{2}E_kP_j-2\gamma_j & E_kP_j-\gamma_j & \frac{1}{2}E_kP_j-2\gamma_j & E_kP_j-\gamma_j & E_kP_j-\gamma_j & \frac{3}{2}E_kP_j
\end{bmatrix}$$

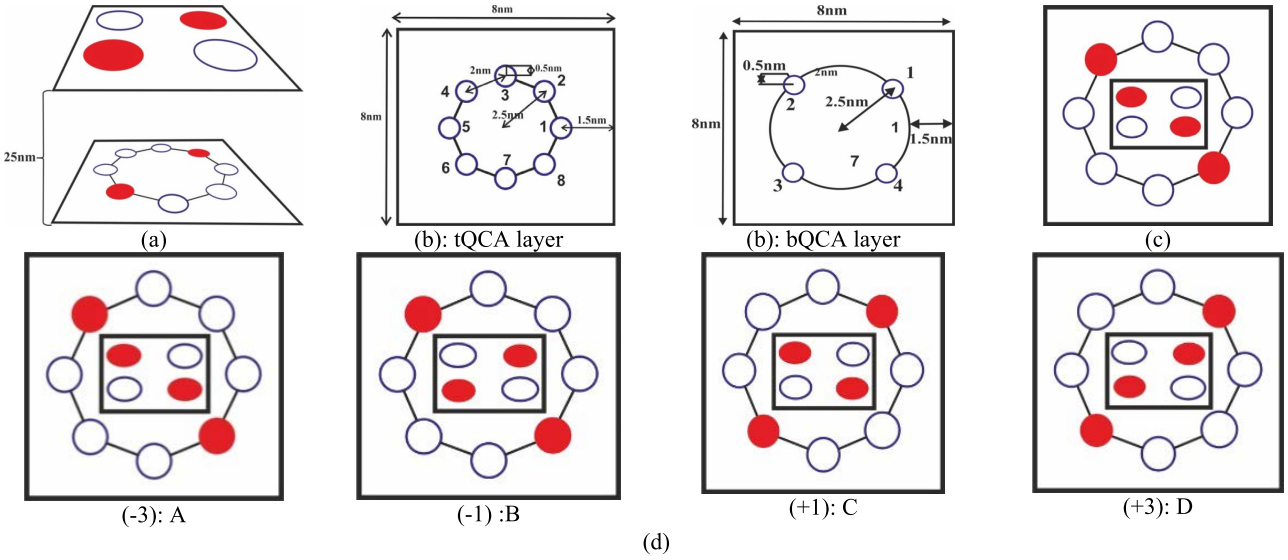

FIGURE 1. (a) QQCA model in [28], (b) specifications of the layers in [28], (c) QQCA cell symbol in [28], and (d) QQCA cell polarization in [28].

The purpose of the integration is to apply the calculated polarizations into each of the QQCA cells.

Figure 1(d) shows the polarization of the QQCA cell, which uses only polarizations -2 and 2 in the first (ternary) layer. These polarizations should be combined with the bQCA polarization to obtain the overall polarization of the QQCA cell. In the first layer, polarizations 0(0°) and 0(90°) are considered as intracellular states.

Input and output drivers are used for input and output integration of polarizations in the QQCA cell. The QQCA cell is designed in such a way that the circuits based on this cell can be implemented in one layer using driver and output [28].

A. INPUT DRIVER DESIGN

The purpose of driving input and output is their integration based on polarization in QQCA. The driver uses two 2×4 decoders with an Enable, and the input of the bQCA layer is used as the decoder input to create the polarization of the ternary layer at the input. In the presented input driver, the first decoder generates a polarization of -2, and the second decoder generates a polarization of 2. If the Enable pin in the proposed circuit is set to -1, decoder 1 is enabled, while if it is set to 1, decoder 2 is activated. It is notable that for the design of the input driver, SETs are used in the binary layer. The SETs are not activated simultaneously for polarizations -1 and $+1$. In fact, these transistors are used at the input to apply information to the ternary layer. Figure 2(a) shows the schematic of the input driver for integrating the input into the QQCA cell.

Table 1 shows the truth table of the input driver. In this study, the SETs in the binary layer are used to specify the polarization in the ternary layer.

B. DESIGN OF OUTPUT DRIVER

For output integration, the QQCA output driver is used. In this driver, the presence of an electron in the SET channel in each layer is equivalent to 1, while the absence of an electron is equivalent to 0.

Two encoders and a decoder are used to realize the integration. To show the polarization in bQCA, two SETs with opposite states are used. These transistors are never activated together, and their simultaneous activation is considered a forbidden state.

The tQCA cell uses four SETs to create polarization in a single cell. These transistors are never activated simultaneously. Figure 2(b) shows the model proposed for the output driver.

Table 2 presents the truth table of the output driver. In this table, the two inputs B and C cannot be identical at the decoder output. This is because B and C are taken from the ternary layer of the QQCA cell. There is an electron in the SETs of QCA cells corresponding to a polarization, while two polarizations never occur simultaneously.

IV. ENERGY OF QQCA CELL

The energy of QQCA cell, like in bQCA and tQCA cells, can be intracellular or extracellular. In the QQCA cell, two layers are used to generate polarization. The first layer contains tQCA, and the second one contains bQCA. The intracellular energy is constant regardless of the polarization. This energy includes internal electrostatic energy, ground state energy, kink energy, and quantum tunneling. Extracellular energy refers to external electrostatic energy. The QQCA cell uses the external electrostatic energy between adjacent cells, as described below.

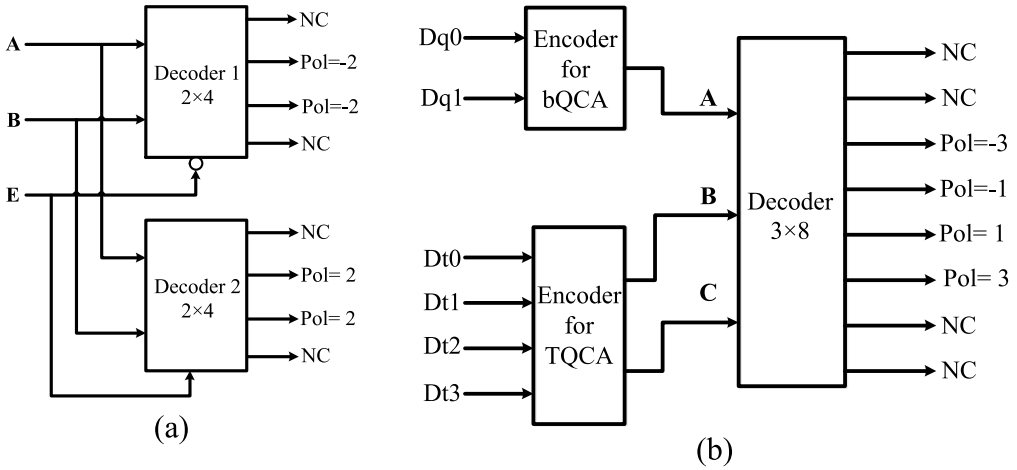

FIGURE 2. Block diagram of (a) the input driver and (b) the output drive in QQCA.

TABLE 1. The truth table of input driver.

Enable	Input binary		Quantum equivalent of input polarization	Output	Connection to transistor corresponding to ternary layer	Quantum equivalent of quaternary polarization
0	A	B	Illegal	Decoder1	------	-----
	0	0		------		
0	0	1	-1	D1	Transistor of Pol. -2	-3
0	1	0	1	D2	Transistor of Pol. -2	-1
0	1	1	Illegal	------	------	
1	0	0	Illegal	Decoder2	-----	-----

1	0	1	-1	D1	Transistor of Pol. 2	1
1	1	0	1	D2	Transistor of Pol. 2	3
1	1	1	Illegal	------	------	------

TABLE 2. The truth table of output driver.

C	B	A	bQCA polarization	tQCA polarization	Q 7	Q 6	Q 5	Q 4	Q 3	Q 2	Q 1	Q 0	Output polarization for QQCA
0	0	0	-1	Illegal	0	0	0	0	0	0	0	1	**Illegal**
0	0	1	1	Illegal	0	0	0	0	0	0	1	0	**Illegal**
0	1	0	-1	-2	0	0	0	0	0	1	0	0	**-3**
0	1	1	1	-2	0	0	0	0	1	0	0	0	**-1**
1	0	0	-1	2	0	0	0	1	0	0	0	0	**1**
1	0	1	1	2	0	0	1	0	0	0	0	0	**3**
1	1	0	-1	Illegal	0	1	0	0	0	0	0	0	**Illegal**
1	1	1	1	Illegal	1	0	0	0	0	0	0	0	**Illegal**

A. EXTERNAL ELECTROSTATIC ENERGY IN QQCA CELLS

Electrostatic energy is the basis of the operation of QCA-based cells. In these cells, no current flows between two cells during the transmission of information from one cell to another. The electrons in an external electrostatic field interact according to Eq. (11) [28].

$$E_{ij} = \frac{1}{4\pi\varepsilon_0\varepsilon_r}\sum_{i=0}^{m}\sum_{j=0}^{n}\frac{q_i q_j}{d_{ij}} \tag{11}$$

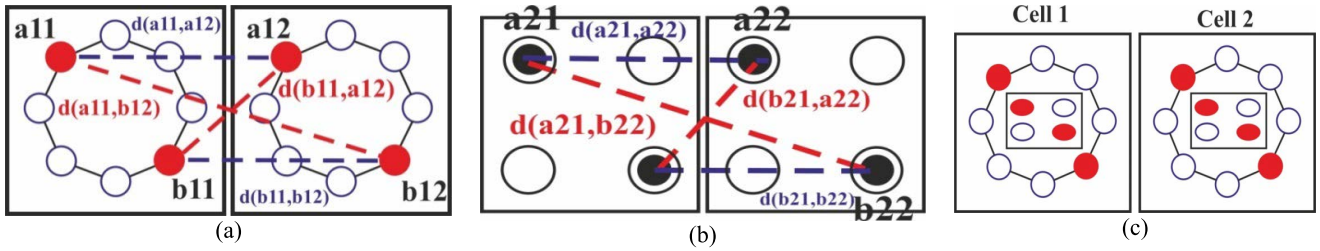

FIGURE 3. Symbolic representation of distances between two QQCA cells in [28]; (a) distances between two ternary cells, (b) distances between binary cells, and (c) symbolic representation of the two QQCA cells.

The distance between the two layers in the QQCA cell is considered to be 25 nm to avoid effective electrostatic interaction between the layers. The method presented in [2] is used to calculate the electrostatic energy between the two cells. For calculating the electrostatic energy of the quaternary cell, the electrostatic energies of the first and second layers are summed. The distances between electrons in two neighboring cells in the first layer (a_{12}, a_{11}), (b_{12}, b_{11}), (b_{12}, a_{11}), and (b_{11}, a_{12}) are calculated, and then, the external electrostatic energy between electrons corresponding to these distances, i.e., E_{e11}, E_{e12}, E_{e13} and E_{e14}, respectively, are determined.

In the next step, the energies resulting from similar labels (E_{e11} and E_{e12}) are summed, as well as those from dissimilar labels (E_{e13} and E_{e14}); the final electrostatic energy of the ternary layer ($E_{t_{tQCA\ layer}}$) is obtained by subtracting these two values as given in Eq. (12).

$$E_{t_{tQCAlayer}} = (E_{e11} + E_{e12}) - (E_{e13} + E_{e14}) \tag{12}$$

Figure 3(a) shows how the distances between electrons in two neighboring cells in the first layer are labeled [28].

In the second layer, the same process as in the first one is followed. The distances between electrons in the second layer of two neighboring cells are (a_{22}, a_{21}), (b_{22}, b_{21}), (b_{22}, a_{21}), and (b_{21}, a_{22}). The external electrostatic energies corresponding to these distances are E_{e21}, E_{e22}, E_{e23}, and E_{e24}, respectively. In the next step, the energies resulting from similar labels (E_{e21} and E_{e22}) are summed, as well as those from dissimilar labels (E_{e13} and E_{e14}); the final electrostatic energy of the second binary layer ($E_{t_{bQCA\ layer}}$) is obtained by subtracting these two values as given in Eq. (13) [28].

$$E_{t_{bQCAlayer}} = (E_{e21} + E_{e22}) - (E_{e23} + E_{e24}) \tag{13}$$

Figure 3(b) shows how the distances between electrons in two neighboring cells in the second layer are labeled. In the final step, to calculate the electrostatic energy in a QQCA cell, the values $|E_{t_{TQCA\ layer}}|$ and $|E_{t_{bQCA\ layer}}|$ are algebraically summed as given in Eq. (14). Figure 3(c) illustrates the symbolic representation of the two QQCA cells [28].

$$|E_{t_{QQCA}}| = |E_{t_{TQCAlayer}}| + |E_{t_{bQCAlayer}}| \tag{14}$$

V. CLOCK IN QQCA

The clock in QQCA is the same as the clock in bQCA, with the following four phases:

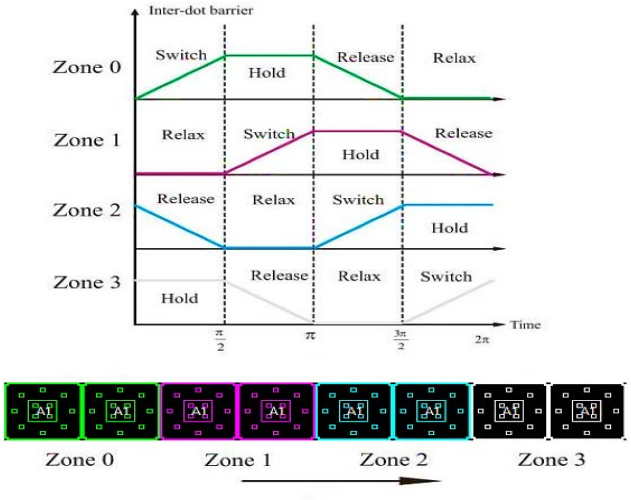

FIGURE 4. Clock in QQCA [28].

- Switch
- Hold
- Release
- Relax

In the zero or Switch phase, the potential of the barrier increases slowly, which reduces the kinetic energy of the electrons in each layer. In the first or Hold phase, the potential of the barrier reaches its maximum, and the kinetic energy of the electrons in each layer is almost zero. In the second or Release phase, the potential of the barrier begins to decrease slowly, and the kinetic energy of the electrons in each layer begins to increase. In the fourth or Relax phase, the potential of the barrier reaches its lowest point, and electrons can easily tunnel into any layer of the QQCA cell. Of course, tunneling only occurs inside the cell, and there is no tunneling from one cell to another. The clocking in QQCA is shown in Figure 4 [28].

VI. POWER DISSIPATION IN QQCA CELL

The power dissipation in a QQCA cell can be examined from two perspectives. First, the power consumption of a three-particle system for quantum computing, and second, the power dissipation of the QQCA cell [28]. Equation 15 calculates power dissipation in a cell in QCA

technology.

$$P_{diss} = \frac{dE}{dt} = -\frac{1}{\tau}(E - E_{ss}) \tag{15}$$

where τ is the time of the Relax phase and change in polarization, E is the expected energy calculated from the measurement of the Hamiltonian matrix (due to the movement of electrons in the potential wells calculated in Eq. 16), and E_{ss} is the thermal equilibrium energy calculated from Eq. 17 [28], [29], [31].

$$E = \frac{h}{2}\vec{\Gamma}\,\vec{\lambda} \tag{16}$$

$$E_{ss} = \frac{\hbar}{2}\vec{\Gamma}\,\vec{\lambda}_{ss} = -(\frac{\hbar\left|\vec{\Gamma}\right|}{2})\tanh(\Delta) \tag{17}$$

where $\hbar$ is the reduced Planck constant, Γ is the magnitude of the energy vector in the x, y, and z directions, $\vec{\lambda}$ is the coefficient vector of the density matrix, and $\vec{\lambda}_{ss}$ is the steady-state coefficient. Equations 18 to 20 have to be calculated for obtaining these parameters [28], [29], [31]. The power dissipation of the QQCA cell is shown in Figure 5.

$$\vec{\Gamma}_i = \frac{Tr\left[\widehat{H}\delta_i\right]}{\hbar}\mathrm{i} = \mathrm{x,y,z} \tag{18}$$

$$\vec{\lambda} = \langle\delta_i\rangle\ \mathrm{i} = \mathrm{x,y,z} \tag{19}$$

$$\vec{\lambda}_{ss} = -\frac{\vec{\Gamma}}{\left|\vec{\Gamma}\right|}\tanh(\Delta), \quad \Delta = \frac{\hbar\left|\vec{\Gamma}\right|}{2K_bT} \tag{20}$$

VII. PROPOSED MAJORITY FUZZY GATE STRUCTURE IN QQCA

In the quantum calculation of QQCA, the polarization is determined from the Hartree-Fock approximation in the form $\{-3, -1, 1, 3\}$. A QQCA cell is a three-particle system, and if the three particles are considered in one layer, the quantum numbers of two identical particles cause instability in the cell and incorrect output of the logic gates.

As explained in Section 2, the QQCA cell has two layers, with the tQCA cell in the first layer and the bQCA cell in the second layer. QQCA polarization was obtained from the algebraic sum of the polarization of these two layers. The purpose of this section is to design QQCA majority fuzzy gates similar to bQCA ones in a single-phase clock.

In the QQCA cell, the circular radius of the potential wells is 2.5 nm, and their distance from the wall is 1.5 nm. The wells in the first and second layers are at 45- and 90-degree angles, respectively.

First, all the states {A B C D} are applied to the inputs of the majority fuzzy gate structure, as shown in Figure 6. The standard majority fuzzy gate is shown in Figure 6a, and the diagonal majority fuzzy gate is shown in Figure 6b. The responses of the two proposed gates as states {A, B, C, D} are given in Table 3. The proposed majority fuzzy gates are the basis for the design of AND and OR gates, which are not plotted for the sake of brevity [42]–[44].

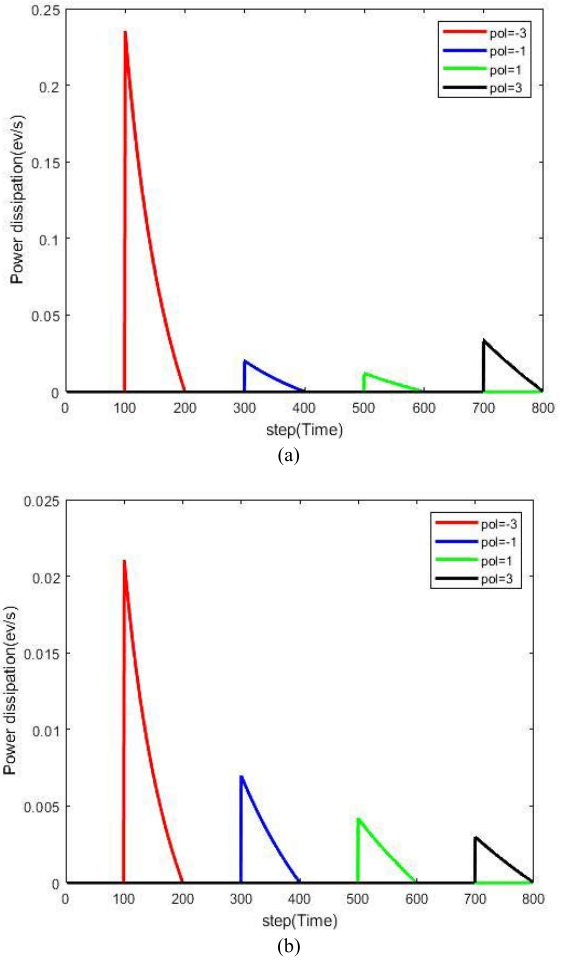

FIGURE 5. a) power dissipation in QQCA for quantum calculation and b) power dissipation of the QQCA [28].

VIII. QQCA SIMULATOR FOR CIRCUIT SIMULATION

In this section, QQCA Sim software is reviewed based on calculations. This software was first introduced in [28], and its functions are similar to computer programs such as tQCA Sim [2] and QCA Designer. The QQCA Sim software can be used to simulate QCA-based quaternary circuits. In this software, the cell size is considered to be 8 nm×8 nm. According to [45], size reduction in QCA technology improves cell performance, and we examine this improvement in metal QCA technology. Based on calculations, the polarization in a quaternary system is calculated as $\{-3, -1, 1, 3\}$. The combination of polarizations of bQCA and tQCA gives the overall polarization.

In this study, a majority fuzzy gate is first proposed by using the QQCA cell and by performing the simulation. Then, this gate is used as the basis for designing AND, OR, and NOT basic gates. An XOR fuzzy gate is implemented to verify the performance of the presented majority fuzzy gate (AND, OR, and NOT basic gates are marked in Figure 8, which shows the implemented XOR fuzzy gate). The majority fuzzy gate based

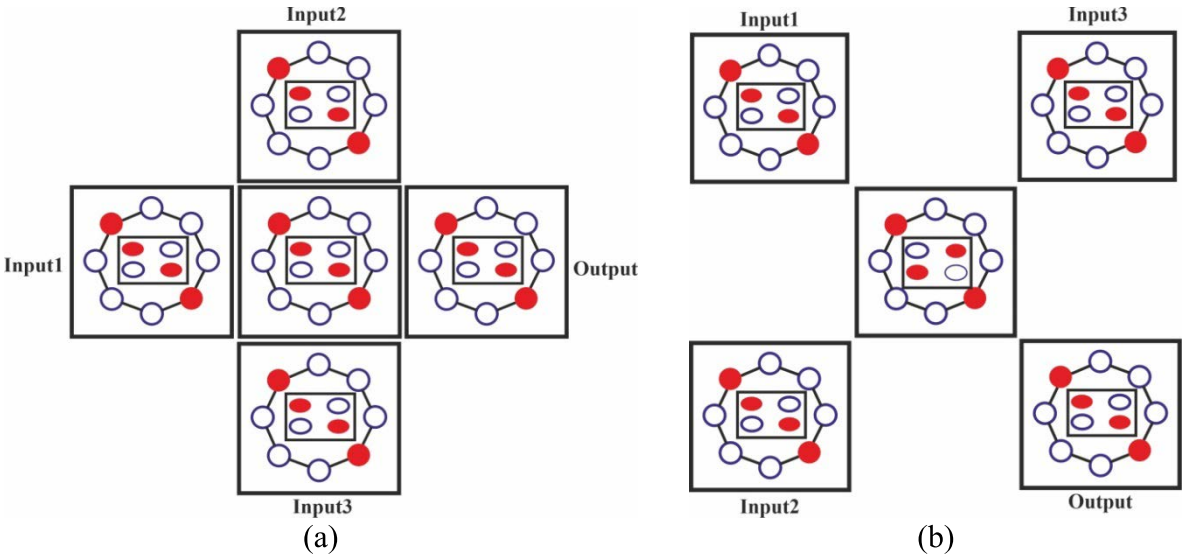

FIGURE 6. (a) standard and (b) diagonal QQCA majority fuzzy gates.

TABLE 3. QQCA majority gate output.

In1	*In2*	*In3*	*Out*	*In1*	*In2*	*In3*	*Out*	*In1*	*In2*	*In3*	*Out*	*In1*	*In2*	*In3*	*Out*
A	A	A	A	B	A	A	A	C	A	A	A	D	A	A	A
A	A	B	A	B	A	B	B	C	A	B	A	D	A	B	**B**
A	A	C	A	B	A	C	A	C	A	C	C	D	A	C	C
A	A	D	A	B	A	D	B	C	A	D	C	D	A	D	D
A	B	A	A	B	B	A	B	C	B	A	A	D	B	A	B
A	B	B	B	B	B	B	B	C	B	B	B	D	B	B	B
A	**B**	**C**	**A**	B	B	C	B	C	B	C	C	**D**	**B**	**C**	**D**
A	B	D	B	B	B	D	B	C	B	D	D	D	B	D	D
A	C	A	A	B	C	A	A	C	C	A	C	D	C	A	C
A	**C**	**B**	**A**	B	C	B	B	C	C	B	C	**D**	**C**	**B**	**D**
A	C	C	C	B	C	C	C	C	C	C	C	D	C	C	C
A	C	D	C	B	C	D	D	C	C	D	C	D	C	D	D
A	D	A	A	B	D	A	B	C	D	A	C	D	D	A	D
A	D	B	B	B	D	B	B	C	D	B	D	D	D	B	D
A	D	C	C	B	D	C	D	C	D	C	C	D	D	C	D
A	D	D	D	B	D	D	D	C	D	D	B	D	D	D	D

on the QQCA cell is simulated by the QQCA Sim software version 1.0.0.1.

A. MAJORITY FUZZY GATE

Based on the QQCA cell model, the structure of the majority fuzzy gate presented in this study is similar to that of the bQCA or tQCA majority fuzzy gate because the two cell models are used in the design. In the majority fuzzy gate, the output response is the state with the most repetitions at the input. To conform to the QCA standard, the majority fuzzy gate is simulated in one clock phase. Figure 7 shows the majority fuzzy gate and results provided by QQCA Sim software. In this figure, the input cell is blue, the middle cell is green, and the output cell is yellow. The comparison of the majority fuzzy gate results in Table 3, and the simulation results show a good agreement, which indicates the accuracy of the calculations.

The QQCA-based gates were simulated in one phase clock to fully conform to the QCA standard.

In the majority fuzzy gate, if one of the inputs remains constant in State A, the quaternary AND function can be implemented; if one of the inputs remains constant in State D, the quaternary OR function can be implemented. To date, quaternary majority fuzzy gates have not been studied.

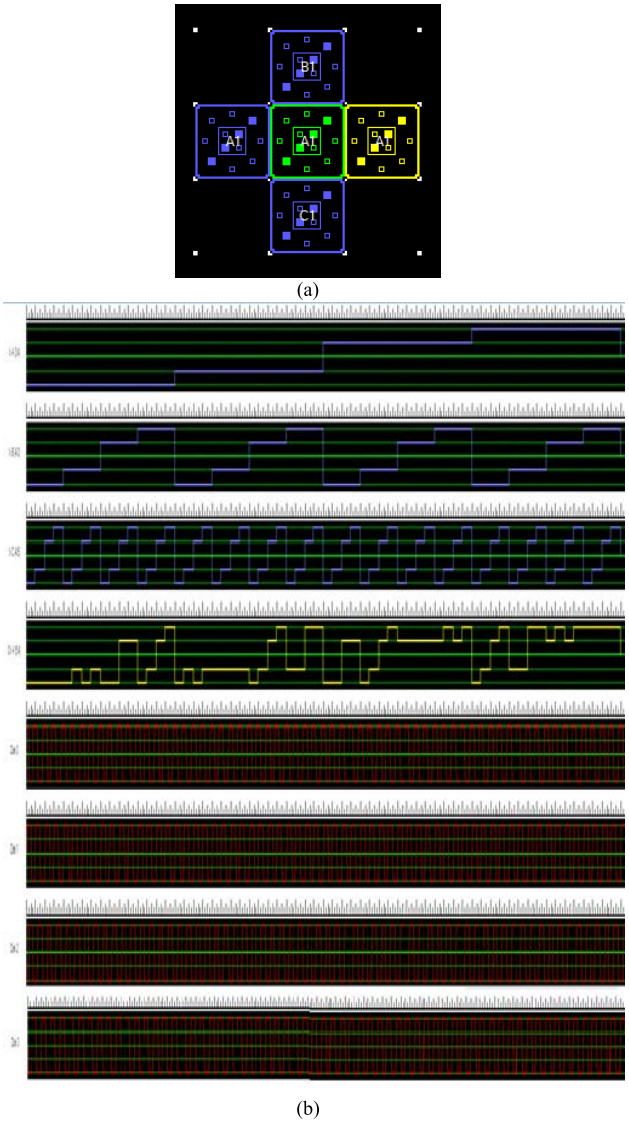

FIGURE 7. Majority fuzzy gate and results provided by QQCA Sim software; (a) majority fuzzy gate, (b) output waveform of the majority fuzzy gate.

Therefore, the proposed gate with Min and Max functions, which are similar to the quaternary AND and OR functions, is compared with its counterparts in CMOS and CNTFET technologies in terms of latency and complexity, as shown in Table 4.

B. IMPLEMENTATION OF XOR FUZZY FUNCTION IN QQCA

The XOR operator consists of a combination of basic operators. A quaternary XOR fuzzy gate has two inputs and in quaternary algebra produces one output according to Eq. 15. In this equation, A and B are the inputs of the XOR fuzzy gate, and y is the output of the gate Designing the quaternary XOR fuzzy gate requires two AND gates, two NOT gates, and one quaternary OR gate.

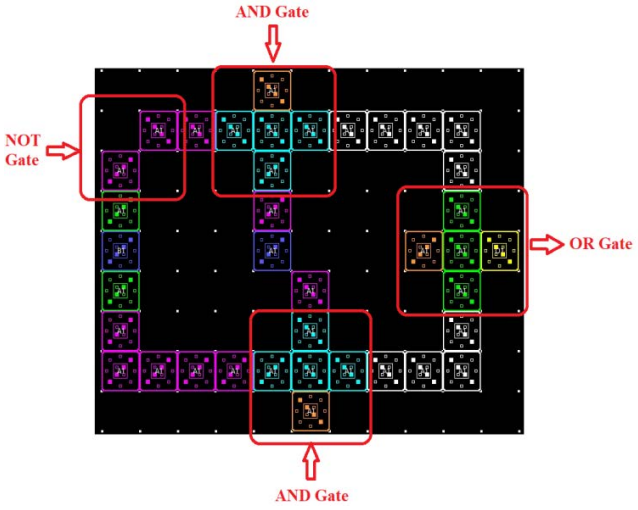

FIGURE 8. Quaternary XOR fuzzy gate.

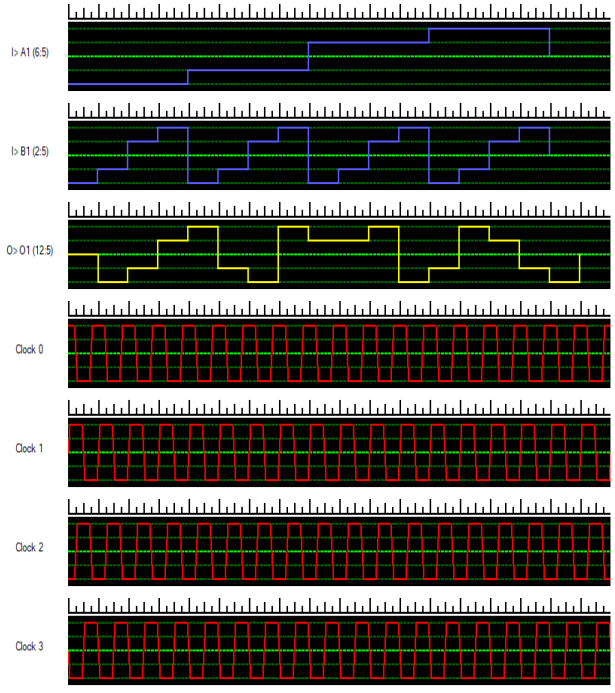

FIGURE 9. The output waveform from the simulation results.

The designed quaternary XOR fuzzy gate using the QQCA cell is shown in Figure 8.

$$y = AB' + A'B \tag{21}$$

The simulation results and the truth table of the XOR fuzzy gate, which uses 38 QQCA cells, are shown in Figure 9. The results demonstrate the correct performance of the proposed XOR fuzzy gate compared to [42], [43].

C. IMPLEMENTATION OF CROSSBAR WITH QQCA CELL

This section simulates a crossbar using a QQCA cell. In QCA-based circuits, crossing wires are one of the most

TABLE 4. Comparison of the proposed majority fuzzy gate with Min and Max functions.

Gate	*Complexity (# Cell)*	*Latency (s)*
Proposed majority fuzzy gate	5	0.25×10^{-12}
NOT Gate + NMIN Gate (CNTFET) [46]	26	34.9×10^{-12}
NOT Gate + NMAX Gate (CNTFET) [46]	26	34.92×10^{-12}
NOT Gate + NMIN Gate (CNTFET) [47]	20	21.85×10^{-12}
NOT Gate + NMAX Gate (CNTFET) [47]	20	16.82×10^{-12}
NOT Gate + NMIN Gate (CMOS) [48]	18	733×10^{-12}
NOT Gate + NMAX Gate (CMOS) [48]	18	704×10^{-12}

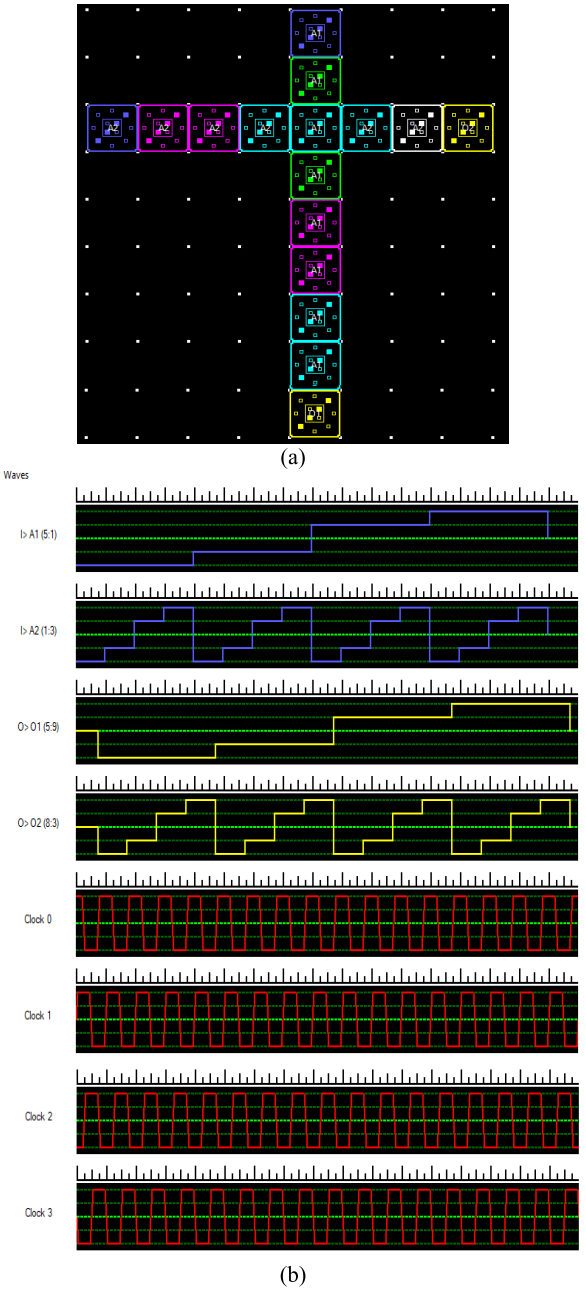

(a)

(b)

FIGURE 10. (a) Structure of cross over, (b) output waveform.

important issues. Crossbar designs using QQCA and bQCA cells are the same. In a crossbar design, the wire-crossing point should have two different clock phases so that the signals on the crossing wires do not interfere with each other. Figure 10 shows the QQCA-based crossbar, its simulation results, and its truth table. In this figure, input signal A1 is transmitted to output O1 and input signal A2 to output O2; this indicates the proper operation of the crossbar, which uses the QQCA cell.

IX. DISCUSSION AND CONCLUSION

In this study, basic quaternary quantum gates were investigated. These gates were based on the QQCA cell model, which is a three-particle structure. Some polarization values were repetitive, so they were omitted, and the final polarization set was obtained as $\{-3\ -1\ 1\ 3\}$. Since including more than two electrons in one layer could result in cell instability, the QQCA cell was presented in two layers to design stable gates. In the QQCA cell, the first layer uses a ternary cell and the second layer uses a binary cell in two-particle and one-particle structures, respectively. In the QQCA cell, the two layers are separated by 25 nm to avoid effective electrostatic interaction between the layers. The size of the cell is 8 nm$\times$8 nm, and the overall polarization of the QQCA cell can be determined as the sum of the polarizations of the layers, as follows: For polarization -3, the polarizations -2 and -1 correspond, respectively, to the ternary and binary layers are summed; for obtaining -1, polarizations -2 and 1 are summed; for obtaining 1, polarizations 2 and -1 correspond, respectively, to the ternary and binary layers are summed; finally, for obtaining 3, polarizations 2 and 1 are summed. Using the QQCA cell, a majority fuzzy gate, an XOR fuzzy gate, and a crossbar structure were designed. The results of the QQCA cell design are in good agreement with those of the quaternary gates designed in CMOS technology, yet designing a logic gate in QQCA is much easier than in CMOS technology. The QQCA-based gates were simulated in one phase clock to fully conform to the QCA standard.

REFERENCES

[1] S. M. Mohaghegh, R. Sabbaghi-Nadooshan, and M. Mohammadi, "Designing ternary quantum-dot cellular automata logic circuits based upon an alternative model," *Comput. Electr. Eng.*, vol. 71, pp. 43–59, Oct. 2018.

[2] S. M. Mohaghegh, R. Sabbaghi-Nadooshan, and M. Mohammadi, "Innovative model for ternary QCA gates," *IET Circuits, Devices Syst.*, vol. 12, no. 2, pp. 189–195, Mar. 2018.

[3] S. Tabrizchi, A. Panahi, F. Sharifi, H. Mahmoodi, and A.-H. A. Badawy, "Energy-efficient ternary multipliers using CNT transistors," *Electronics*, vol. 9, no. 4, p. 643, Apr. 2020.

[4] A. K. Pramanik, D. Bhowmik, J. Pal, P. Sen, A. K. Saha, and B. Sen, "Towards the realization of regular clocking-based QCA circuits using genetic algorithm," *Comput. Electr. Eng.*, vol. 97, Jan. 2022, Art. no. 107640.
[5] F. Salimzadeh and S. R. Heikalabad, "Design of a novel reversible structure for full adder/subtractor in quantum-dot cellular automata," *Phys. B, Condens. Matter*, vol. 556, pp. 163–169, Mar. 2019.
[6] E. Alkaldy, A. H. Majeed, M. S. Zainal, and D. M. Nor, "Optimum multiplexer design in quantum-dot cellular automata," 2020, *arXiv:2002.00360*.
[7] M. Hayati and A. Rezaei, "Design of a new optimized universal logic gate for quantum-dot cellular automata," *IETE J. Res.*, pp. 1–7, 2019, doi: 10.1080/03772063.2019.1643262.
[8] I. Gassoumi, L. Touil, and A. Mtibaa, "An efficient QCA-based full adder design with power dissipation analysis," *Int. J. Electron. Lett.*, 2022, doi: 10.1080/21681724.2021.2025440.
[9] I. L. Bajec, N. Zimic, and M. Mraz, "The ternary quantum-dot cell and ternary logic," *Nanotechnology*, vol. 17, no. 8, p. 1937, 2006.
[10] L. Wang and G. Xie, "A novel XOR/XNOR structure for modular design of QCA circuits," *IEEE Trans. Circuits Syst. II, Exp. Briefs*, vol. 67, no. 12, pp. 3327–3331, Dec. 2020.
[11] R. Singh and D. K. Sharma, "Design of efficient multilayer RAM cell in QCA framework," *Circuit World*, vol. 47, no. 1, pp. 31–41, May 2020.
[12] D. Mukhopadhyay and P. Dutta, "A study on energy optimized 4 dot 2 electron two dimensional quantum dot cellular automata logical reversible flip-flops," *Microelectron. J.*, vol. 46, no. 6, pp. 519–530, Jun. 2015.
[13] F. Sill Torres, R. Wille, P. Niemann, and R. Drechsler, "An energy-aware model for the logic synthesis of quantum-dot cellular automata," *IEEE Trans. Comput.-Aided Design Integr. Circuits Syst.*, vol. 37, no. 12, pp. 3031–3041, Dec. 2018.
[14] B. Das, M. Mahmood, M. Rabeya, and R. Bardhan, "An effective design of 2 : 1 multiplexer and 1 : 2 demultiplexer using 3-dot QCA architecture," in *Proc. Int. Conf. Robot., Elect. Signal Process. Techn. (ICREST)*, Jan. 2019, pp. 570–575.
[15] M. Ghosh, D. Mukhopadhyay, and P. Dutta, "Design of an arithmetic circuit using non-reversible adders in 2 dot 1 electron QCA," *Microsyst. Technol.*, vol. 25, no. 5, pp. 1719–1729, May 2019.
[16] A. Sarker, M. Badrul, and A. Newaz, "Design of 1-bit comparator using 2 dot 1 electron quantum-dot cellular automata," *Int. J. Adv. Comput. Sci. Appl.*, vol. 8, no. 3, pp. 481–485, 2017.
[17] M. Ghosh, D. Mukhopadhyay, and P. Dutta, "A 2 dot 1 electron quantum cellular automata based parallel memory," in *Information Systems Design and Intelligent Applications* (Advances in Intelligent Systems and Computing), vol. 339, J. Mandal, S. Satapathy, M. K. Sanyal, P. Sarkar, and A. Mukhopadhyay, Eds. New Delhi, India: Springer, 2015, doi: 10.1007/978-81-322-2250-7_63.
[18] M. Ghosh, D. Mukhopadhyay, and P. Dutta, "Energy efficient designing approach of flip-flops using 2-dot 1-electron QCA," in *Computational Intelligence, Communications, and Business Analytics* (Communications in Computer and Information Science), vol. 1030, J. Mandal, S. Mukhopadhyay, P. Dutta, and K. Dasgupta, Eds. Singapore: Springer, 2019, doi: 10.1007/978-981-13-8578-0_38.
[19] K. Datta, D. Mukhopadhyay, and P. Dutta, "Comprehensive design and analysis of Gray code counters using 2-dimensional 2-dot 1-electron QCA," *Microsyst. Technol.*, vol. 28, pp. 447–465, Mar. 2018.
[20] R. Akbari-Hasanjani, R. Sabbaghi-Nadooshan, and M. R. Tanhayi, "New polarization and power calculations with error elimination in ternary QCA," *Comput. Electr. Eng.*, vol. 96, Dec. 2021, Art. no. 107557.
[21] M. A. Tehrani, S. Bahrami, and K. Navi, "A novel ternary quantum-dot cell for solving majority voter gate problem," *Appl. Nanosci.*, vol. 4, no. 3, pp. 255–262, Mar. 2014.
[22] R. Akbari-Hasanjani and R. Sabbaghi-Nadooshan, "Innovation quinary and *n*-value toward fuzzy logic QCA cell design," *Adv. Theory Simul.*, vol. 5, no. 2, Feb. 2022, Art. no. 2100304.
[23] S. F. Kamali, S. Tabrizchi, S. Mohammadyan, M. Rastgoo, and K. Navi, "Designing positive, negative and standard gates for ternary logics using quantum dot cellular automata," *Comput. Electr. Eng.*, vol. 83, May 2020, Art. no. 106590.
[24] K. Das, D. De, and M. De, "Modified ternary Karnaugh map and logic synthesis in ternary quantum dot cellular automata," *IETE J. Res.*, vol. 62, no. 6, pp. 774–785, Nov. 2016.
[25] P. Pain, A. Sadhu, K. Das, and M. R. Kanjilal, "Physical proof and simulation of ternary logic gate in ternary quantum dot cellular automata," in *Computational Advancement in Communication Circuits and Systems* (Lecture Notes in Electrical Engineering), vol. 575, K. Maharatna, M. Kanjilal, S. Konar, S. Nandi, and K. Das, Eds. Singapore: Springer, 2020, doi: 10.1007/978-981-13-8687-9_34.
[26] A. Simonetta and M. C. Paoletti, "Designing digital circuits in multi-valued logic," *Int. J. Adv. Sci., Eng. Inf. Technol.*, vol. 8, no. 4, pp. 1166–1172, 2018.
[27] Z. Toffano and F. Dubois, "Interpolating binary and multivalued logical quantum gates," *Multidisciplinary Digit. Publishing Inst. Proc.*, vol. 2, no. 4, p. 152, 2017.
[28] R. Akbari-Hasanjani and R. Sabbaghi-Nadooshan, "Design and simulation of innovative QCA quaternary logic gates," *Adv. Theory Simul.*, vol. 4, no. 9, Sep. 2021, Art. no. 2100069.
[29] J. Timler and C. S. Lent, "Power gain and dissipation in quantum-dot cellular automata," *J. Appl. Phys.*, vol. 91, no. 2, pp. 823–831, Jan. 2002.
[30] P. D. Tougaw and C. S. Lent, "Dynamic behavior of quantum cellular automata," *J. Appl. Phys.*, vol. 80, no. 8, pp. 4722–4736, Oct. 1996.
[31] S. Srivastava, S. Sarkar, and S. Bhanja, "Estimation of upper bound of power dissipation in QCA circuits," *IEEE Trans. Nanotechnol.*, vol. 8, no. 1, pp. 116–127, Jan. 2009.
[32] S. Srivastava, A. Asthana, S. Bhanja, and S. Sarkar, "QCAPro—An error-power estimation tool for QCA circuit design," in *Proc. IEEE Int. Symp. Circuits Syst. (ISCAS)*, May 2011, pp. 2377–2380.
[33] W. Liu, S. Srivastava, L. Lu, M. O'Neill, and E. E. Swartzlander, "Are QCA cryptographic circuits resistant to power analysis attack?" *IEEE Trans. Nanotechnol.*, vol. 11, no. 6, pp. 1239–1251, Nov. 2012.
[34] A. N. Bahar, F. Ahmad, S. Wani, S. Al-Nisa, and G. M. Bhat, "New modified-majority voter-based efficient QCA digital logic design," *Int. J. Electron.*, vol. 106, no. 3, pp. 333–348, Mar. 2019.
[35] M. Macucci, M. Gattobigio, L. Bonci, G. Iannaccone, F. E. Prins, C. Single, G. Wetekam, and D. P. Kern, "A QCA cell in silicon-on-insulator technology: Theory and experiment," *Superlattices Microstruct.*, vol. 34, nos. 3–6, pp. 205–211, Sep. 2003.
[36] M. Hofmann, L. Weidenfeller, S. Supreeti, S. Mechold, M. Holz, C. Reuter, S. Sinzinger, E. Manske, and I. W. Rangelow, "Mix-and-match lithography and cryogenic etching for NIL template fabrication," *Microelectron. Eng.*, vol. 224, Mar. 2020, Art. no. 111234.
[37] P. Gao, M. Pu, X. Ma, X. Li, Y. Guo, C. Wang, Z. Zhao, and X. Luo, "Plasmonic lithography for the fabrication of surface nanostructures with a feature size down to 9 nm," *Nanoscale*, vol. 12, no. 4, pp. 2415–2421, 2020.
[38] W. Chen and H. Ahmed, "Fabrication of 5–7 nm wide etched lines in silicon using 100 keV electron-beam lithography and polymethylmethacrylate resist," *Appl. Phys. Lett.*, vol. 62, no. 13, pp. 1499–1501, Mar. 1993.
[39] B. Päivänranta, A. Langner, E. Kirk, C. David, and Y. Ekinci, "Sub-10 nm patterning using EUV interference lithography," *Nanotechnology*, vol. 22, no. 37, Sep. 2011, Art. no. 375302.
[40] M. B. Haider, J. L. Pitters, G. A. DiLabio, L. Livadaru, J. Y. Mutus, and R. A. Wolkow, "Controlled coupling and occupation of silicon atomic quantum dots at room temperature," *Phys. Rev. Lett.*, vol. 102, no. 4, Jan. 2009, Art. no. 046805.
[41] M. B. Haider, J. L. Pitters, G. A. DiLabio, L. Livadaru, J. Y. Mutus, and R. A. Wolkow, "Controlled coupling and occupation of silicon atomic quantum dots at room temperature," *Phys. Rev. Lett.*, vol. 102, no. 4, Jan. 2009, Art. no. 046805.
[42] S. N. Chowdhury, A. Faiyaz, and K. M. Ishtiak, "Formulation and design of useful logic gates using quaternary algebra," *Int. J. Sci. Eng. Res.*, vol. 6, no. 1, pp. 1–7, Jan. 2015.
[43] I. Jahangir, D. M. N. Hasan, S. Islam, N. A. Siddique, and M. M. Hasan, "Development of a novel quaternary algebra with the design of some useful logic blocks," in *Proc. 12th Int. Conf. Comput. Inf. Technol.*, Dec. 2009, pp. 197–202.
[44] N. K. Naware, D. S. Khurge, and S. U. Bhandari, "Review of quaternary algebra & its logic circuits," in *Proc. Int. Conf. Comput. Commun. Control Autom.*, Feb. 2015, pp. 969–973.
[45] R. Akbari-Hasanjani and R. Sabbaghi-Nadooshan, "New design of binary to ternary converter," *IETE J. Res.*, pp. 1–12, 2021, doi: 10.1080/03772063.2021.1886881.
[46] S. A. Ebrahimi, M. R. Reshadinezhad, A. Bohlooli, and M. Shahsavari, "Efficient CNTFET-based design of quaternary logic gates and arithmetic circuits," *Microelectron. J.*, vol. 53, pp. 156–166, Jul. 2016.
[47] F. Sharifi, M. H. Moaiyeri, K. Navi, and N. Bagherzadeh, "Ultra-low-power carbon nanotube FET-based quaternary logic gates," *Int. J. Electron.*, vol. 103, no. 9, pp. 1524–1537, Sep. 2016.
[48] R. C. G. da Silva, H. Boudinov, and L. Carro, "A novel voltage-mode CMOS quaternary logic design," *IEEE Trans. Electron Devices*, vol. 53, no. 6, pp. 1480–1483, Jun. 2006.

REZA AKBARI-HASANJANI received the B.Sc., M.Sc., and Ph.D. degrees in electrical engineering from Central Tehran Branch, Islamic Azad University, Tehran, Iran, in 2012, 2015, and 2022, respectively. His research interests include nanocomputing, reversible gates, multiple-value logic, and QCA.

REZA SABBAGHI-NADOOSHAN received the B.S. and M.S. degrees in electrical engineering from the Iran University of Science and Technology, Tehran, Iran, in 1991 and 1994, respectively, and the Ph.D. degree in electrical engineering from the Science and Research Branch, Islamic Azad University, Tehran, in 2010. He is currently an Associate Professor with the Department of Electronics in Central Tehran Branch, Islamic Azad University. He has published more than 100 research papers in various international journals and conferences. His research interests include multiple value logic, QCA, and nanocomputing. He is on the panel of reviewers for various international journals.

MAJID HAGHPARAST received the B.Sc., M.Sc., and Ph.D. degrees in computer engineering, in 2003, 2006, and 2009, respectively. Since 2007, he has been affiliated with the Computer Engineering Faculty, IAU University, Tehran, where he was an Associate Professor. From April 2017 to January 2018, he has conducted his sabbatical with Johannes Kepler University, Linz, Austria, where he was also a Research Fellow. He is on the panel of reviewers for various international journals. Since September 2021, he has been with the Faculty of Information Technology, University of Jyväskylä, Jyväskylä, Finland. He has published more than 100 research papers in various international journals and conferences. He is also an Associate Editor of the *Cluster Computing* (Springer).